Exploiting the Richness of Multi-Component Data: a Time-Dependent Polarization-Based Fwi Approach

Serge Sambolian, Romain Brossier, Ludovic Métivier

Exploiting the richness of multi-component data: a time-dependent polarization-based FWI approach

S. Sambolian[1*], R. Brossier[1], L. Métivier[1,2]

[1] Univ. Grenoble Alpes, ISTerre, F-38058 Grenoble, France
[2] CNRS, Univ. Grenoble Alpes, LJK, F-38058 Grenoble, France

January 14, 2022

Main objectives

Recasting polarization-based multi-component inversion in a time-domain compatible framework. Showing, through a numerical example, the superior robustness of the proposed approach with respect to phase and amplitude ambiguities compared to more conventional approaches.

New aspects covered

Introducing a strategy for evaluating the distance between polarization states in the time-frequency domain. Presenting the associated misfit function and adjoint sources. Application to a realistic case study with a direct comparison against the classical multi-component full waveform inversion.

Summary (200 words)

Ocean-bottom acquistions are emerging as the go-to strategy for marine surveys. One of their major advantage is the multi-component data accessibility. Commonly, multi-component data are independently inverted in an uncorrelated manner. The relationship between particle motion recorded along different directions could be exploited through polarization. Polarization attributes could serve as a remedy for the ill-posedness of FWI or serve directly as objective measures due to their insensitivity to phase and amplitude ambiguities. In this study, a previously proposed intrinsic polarization-based misfit function for frequency-domain full waveform inversion (FWI) is recasted under a time-domain compatible framework. Through a numerical example on a realistic synthetic example, the conventional and proposed strategies are compared. The obtained results confirm the superior robustness of the polarization-based objective function.

Exploiting the richness of multi-component data: a time-dependent polarization-based FWI approach

Introduction

Over the last decade, a plethora of researches around full waveform inversion (FWI) were conducted (Virieux et al., 2017). Its high resolution power settles it as the standard imaging method both in industrial and academic communities, for exploration as well as for global and deep crustal scale imaging. At different scales, FWI produces satisfactory results in case studies, particularly when acquisitions are well designed. In marine settings, ocean-bottom acquisitions are emerging as the favorable choice. Ocean-bottom seismometers (OBS) offer a favorable signal-to-noise ratio at low frequency and their deployment flexibility lead to areal acquisitions that foster the undershooting of sought structures (Shen et al., 2018). Another advantage, serving as the main point of this the study, is multi-component data accessibility along the seabed through nodes (OBN) or cables (OBC).

For such data, usually only mono-component data (the pressure recorded by the hydrophone or the particle velocity recorded by the vertical component of the geophone) are inverted in the acoustic approximation. The rest of the recorded 4C data, which in most cases does not offer additional constraints on the the P-wave velocity, is disregarded due to a much needed exhaustive data processing for denoising and eliminating unwanted wave conversions. Conversely, when both P-wave and S-wave velocity models are reconstructed jointly, inverting all geophone components data becomes crucial in order to decouple the parameters (Sears et al., 2008; Prieux et al., 2013; Vigh et al., 2014; Cao et al., 2021).

The most straightforward and common strategy for inverting multi-component data consists of independently comparing observed and simulated data under any chosen metric and summing the quantified mismatch of each component without any correlation between them. The correlation between the latter could be exploited for extracting polarization attributes like ellipticity and directionality which in turn serve as alternative observables (Hu and Menke, 1992, among others, used tilt instead traveltimes). In fact, polarization attributes are independent of phase and amplitude ambiguities commonly faced in FWI problems due to incomplete physics at the modeling stage, poor initial guesses of the subsurface parameters and erroneous estimated source wavelet. As a remedy for the ill-posedness of FWI, Charara and Barnes (2019) suggested constraining its data space through a polarization-based covariance matrix. Valensi et al. (2015) revamped the FWI problem by replacing the classical misfit function with an intrinsic metric that evaluates polarization states mismatch.

In this study, we recast under a time-domain framework the formulation originally proposed by Valensi et al. (2015) for frequency-domain FWI. Through a time-frequency domain analysis, time-dependent polarization states are computed on a sequence of short time windows on which the signal is assumed to be stationary (Jurkevics, 1988). We recap the definition of polarization states and present our recipe for inverting multi-component data. In order to demonstrate its added value, even when only P-wave velocity is reconstructed under the acoustic approximation, the approach is applied to a 2D synthetic case where wrong subsurface parameters and physics are used during FWI. The comparison with results obtained using a classical approach illustrates the interest of using a polarization-based inversion.

Polarization-based misfit function in time-domain FWI

We define polarization as a physical attribute that describes the properties of particle motion through the relationship between the different directional measurements of a sensor. Across this study, we assume that multi-component data refer to particle velocity or displacement measurements and that the vertical component of the geophone is perpendicular to the surface while pointing towards the earth center. We introduce a second-order tensor $\mathscr{P}$ obtained through a dyadic product of a monochromatic vectorial signal $\mathbf{v}$, $\mathscr{P} = \mathbf{v}\mathbf{v}^t$, where ^{t} denotes the conjugate transpose operator. In fact, $\mathscr{P}$ is the polarization tensor encompassing mono-component auto-correlations along the diagonal and cross-correlation between the different components elsewhere. In order to define polarization states in an intuitive physical and geometrical manner, we assume for the rest of the development that $\mathbf{v}$ is a bivariate signal. We stress the fact that this recipe is also valid for three component data. As described by Valensi et al. (2015), the 2×2 polarization tensor is decomposed using the three Pauli matrices $\mathbf{P}$ as follows

$$\mathscr{P} = \begin{bmatrix} v_x v_x^* & v_x v_z^* \\ v_z v_x^* & v_z v_z^* \end{bmatrix} = \alpha_0 \mathbf{I} + \alpha_1 \mathbf{P}_1 + \alpha_2 \mathbf{P}_2 + \alpha_3 \mathbf{P}_3, \tag{1}$$

where * denotes the complex conjugation operator and α the so-called Stokes parameters that describe a polarization state. The Stokes parameters could be directly calculated from the vectorial signal with

$$\alpha_0 = v_x v_x^* + v_z v_z^*,\ \alpha_1 = v_x v_x^* - v_z v_z^*,\ \alpha_2 = v_x v_z^* + v_z v_x^*,\ \alpha_3 = i(v_z v_x^* - v_x v_z^*). \tag{2}$$

From the above equation, we can recognize that α_0 quantifies the total energy (unity when the signal is normalized), the second Stoke parameter α_1 describes the linear polarization along the horizontal and vertical directions (ranging from 1 to -1) while α_2 describes the polarization along the 45°-135° direction line and α_3 the degree of ellipticity (ranging from clockwise to counter-clockwise circular polarization). For bivariate cases, the normalized Stoke vector $\mathbf{s}(P)$ associated with a polarization state P can be represented in three-dimension Cartesian coordinates on the Poincaré sphere (Figure 1).

In the context of FWI, two polarization states (observed and simulated data) are represented on the Poincaré sphere where the length of the geodesic curve linking them serves as the distance in the objective function. The latter is estimated by calculating the angle between their corresponding Stokes vectors. The difference between our proposed recipe and the one developed by Valensi et al. (2015) is the calculation of the Stokes parameters in the time-frequency domain. We assume that the signal is locally stationary and that a distinct polarization state could be defined across a time-window centered on t. The polarization objective function $\mathscr{C}$ for a source-receiver pair is rewritten as

$$\mathscr{C}[\mathbf{m}] = \int_t f[t]\, dt, \quad \text{with} \quad f[t] = \int_\omega \left(\frac{1}{\pi}\arccos(S[\omega])\right)^2 d\omega \tag{3}$$

$$\text{and} \quad S[\omega] = \frac{\mathbf{s}(P^o).\mathbf{s}(P^c)}{\|\mathbf{s}(P^o)\|.\|\mathbf{s}(P^c)\|} \approx \frac{\alpha_1^o[\omega]\alpha_1^c[\omega] + \alpha_2^o[\omega]\alpha_2^c[\omega] + \alpha_3^o[\omega]\alpha_3^c[\omega]}{\alpha_0^o[\omega]\alpha_0^c[\omega] + \varepsilon}, \tag{4}$$

where $f[t]$ is an arbitrary time-dependent function and $\mathbf{m}$, ω denote the subsurface parameters and frequency, respectively. A water-level parameter ε is introduced in the denominator of the normalized scalar product $S[\omega]$ to avoid degenerate cases occuring when the signal is null in either the observed or simulated data. We point out the fact that equation 3 can be written for n-dimensional cases using particle motion directly (Valensi et al., 2015). Once calculated, the two adjoint sources needed for minimizing $\mathscr{C}$ are transformed back from the time-frequency domain through the adjoint of the short-time Fourier transformer employed on the data (e.g. Gabor or Stockwell transforms).

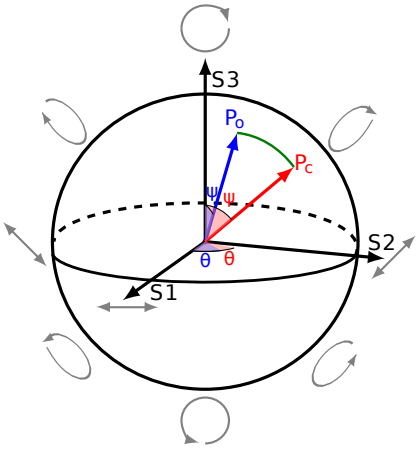

Figure 1 *Poincaré sphere representation. Main polarization states at poles denoted by gray arrows. Two polarization states P_o (blue arrow) and P_c (red arrow) are plotted on the sphere using their Stokes parameters. The azimuth θ and latitude angles ψ correspond to two times the tilt and ellipticity angles of particle motion. The distance between the polarization states is defined by the green geodesic.*

Application to the 2D Valhall synthetic case study

We assess the added value of the aforementioned recipe on the 2D Vallhall case study. A synthetic noise-free dataset is generated in the models of Figure 2. We use a fixed-spread OBS acquisition with a total of 32 sources located at 25 m depth and recorded by 351 nodes deployed at the seabed. The source wavelet is a 8 Hz dominant frequency Ricker that is low-cut filtered to reject energy below 2.5 Hz. We perform two inversions using a conventional multi-component FWI and the proposed polarization-based recipe. Even though the observed data are obtained through a visco-acoustic engine, a mono-parameter inversion for velocity is performed under the acoustic approximation. The motivation behind omitting the effect of attenuation while starting from a smooth version of velocity and a density derived through Gardner's relation (Figure 3a-b) is worsening both phase and amplitude ambiguities in the inversion beyond velocity-related time-shifts and impedance mismatches that could be remedied through an exhaustive

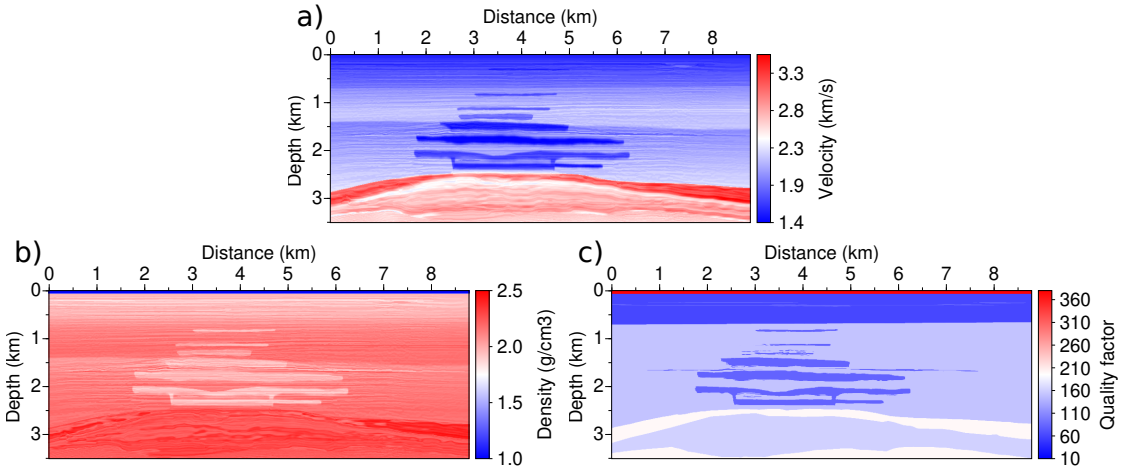

Figure 2 *Valhall synthetic models. (a) P-wave velocity, (b) density and (c) quality factor.*

workflow. We note that no processing is done on the full 9 seconds recordings. The polarization-based approach is insensitive to source wavelet errors; however, an estimated wavelet through linear deconvolution in the initial model is used in both cases in order to have comparable data and tune the width of the Gabor window function with respect to its dominant frequency (shifted as a result of ignoring attenuation). In figure 3c-d, a comparison of the observed and synthetic data at the initial stage for the first OBS is presented. The latter shows logically missing reflected events and a mismatch at intermediate to long offsets where cycle-skipping imprints are present around the first-arrivals that propagated in the strongly attenuative first kilometer and in the deeper gas-rich layers. We use a depth preconditioned l-BFGS and the gradient is locally smoothed with adaptable correlation lengths depending on the velocity.

The reconstructed models using both approaches are presented in Figure 4. The velocity model obtained through conventional FWI contains many artifacts, acquisition imprints are seen below the seabed and more complex erroneous updates are present in deeper parts (Figure 4a). On the other hand, the reconstructed velocity model using the proposed approach does not contain any of the previously mentioned artifacts (Figure 4b), the majority of the structures are well recovered in a sharp manner. We note that despite the near perfect reconstruction, recovering precise velocity contrasts, especially in the deep part, is extremely challenging. The latter is due to being driven by impedance since density serves as a passive parameter in the inversion. The comparison between the observed and simulated data in both models (Figure 4c-d) depicts clear waveform discrepancy in the conventional FWI case. Reflections events are generated by the erroneously updated structures and long-offset arrivals are completely mismatched. The superiority of the proposed recipe is confirmed in the data comparison (Figure 4e-f) where the seismogram, apart from very-short offsets due to poor illumination on the sides, match well.

Conclusion and perspectives

We introduce a time-domain compatible recipe for polarization-based multi-component inversion. The proposed misfit function, more robust to amplitude and phase ambiguities, provides a far more reliable reconstruction on a realistic numerical example. We note that the computational overhead compared to conventional FWI is only associated to the time-frequency transform employed. In future publications, a more thorough description of the method will be presented along with an application on 3D field data.

Acknowledgements

Authors warmly thank Raphael Valensi for inspiring insights on polarization. The authors also wish to thank Jian Cao and Peng Yong for fruitful discussions. This study was partially funded by the SEISCOPE consortium (http://seiscope2.osug.fr), sponsored by AKERBP, CGG, CHEVRON, EQUINOR, EXXONMOBIL, JGI, SHELL, SINOPEC, SISPROBE and TOTAL. This study was granted access to the HPC resources of CIMENT infrastructure (https://ciment.ujf-grenoble.fr) and CINES/IDRIS/TGCC under the allocation 046091 made by GENCI.

References

Cao, J., Brossier, R., Górszczyk, A., Métivier, L. and Virieux, J. [2021] 3D multi-parameter full-waveform inversion for ocean-bottom seismic data using an efficient fluid-solid coupled spectral-element solver. *Geophysical Journal International*, **in press**.

Charara, M. and Barnes, C. [2019] Constrained Full Waveform Inversion for Borehole Multicomponent Seismic Data. *Geosciences*, **9**(1), 45.

Hu, G. and Menke, W. [1992] Formal inversion of laterally heterogeneous velocity structure from P-wave polar-

ization data. *Geophysical Journal International*, **110**, 63–69.
Jurkevics, A. [1988] Polarization analysis of three-component array data. *Bulletin of the Seismological Society of America*, **78**(5), 1725–1743.
Prieux, V., Brossier, R., Operto, S. and Virieux, J. [2013] Multiparameter full waveform inversion of multicomponent OBC data from Valhall. Part 2: imaging compressional and shear-wave velocities. *Geophysical Journal International*, **194**(3), 1665–1681.
Sears, T., Singh, S. and Barton, P. [2008] Elastic full waveform inversion of multi-component OBC seismic data. *Geophysical Prospecting*, **56**(6), 843–862.
Shen, L., Ahmed, I., Brenders, A., Dellinger, J., Etgen, J. and Michell, S. [2018] Full-waveform inversion: the next leap forward in subsalt imaging. *The Leading Edge*, **January**, 76b1–67b6.
Valensi, R., Brossier, R., Baltazart, V., Leparoux, D., Bretaudeau, F. and Côte, P. [2015] A New Kind of Polarization-based Misfit Function -Theoretical Formulation and Application to Full Waveform Inversion. In: *77th EAGE Conference and Exhibition*. European Association of Geoscientists & Engineers.
Vigh, D., Jiao, K., Watts, D. and Sun, D. [2014] Elastic full-waveform inversion application using multicomponent measurements of seismic data collection. *Geophysics*, **79**(2), R63–R77.
Virieux, J., Asnaashari, A., Brossier, R., Métivier, L., Ribodetti, A. and Zhou, W. [2017] An introduction to Full Waveform Inversion. In: Grechka, V. and Wapenaar, K. (Eds.) *Encyclopedia of Exploration Geophysics*, Society of Exploration Geophysics, R1–1–R1–40.

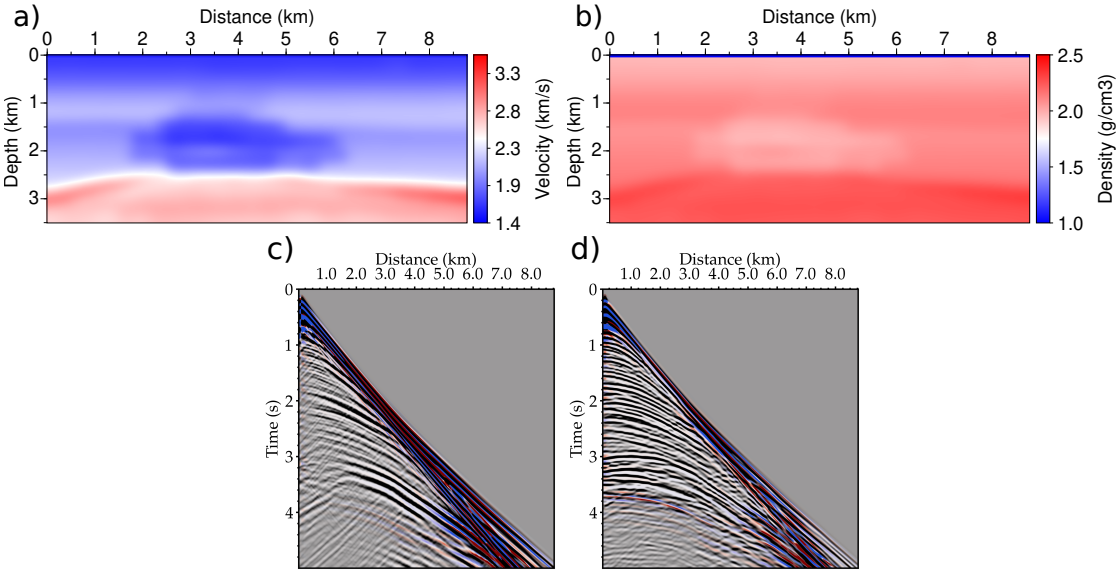

Figure 3 *(a) Initial P-wave velocity guess. (b) Density derived through Gardner's relation. (c-d) Horizontal and vertical particle velocity comparison at the initial stage between exact visco-acoustic data (black and white) and simulated data in (a) and (b) under an acoustic approximation (red and blue).*

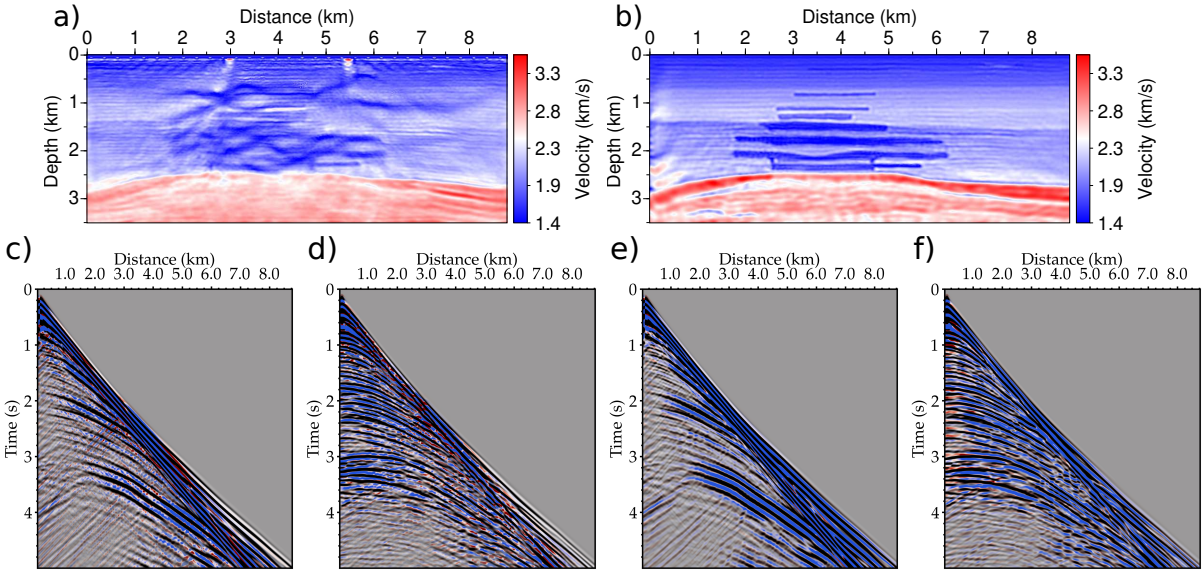

Figure 4 *(a-b) Inverted P-wave velocity using conventional FWI and polarization-based misfit, respectively. (c-d) Horizontal and vertical particle velocity comparison between exact visco-acoustic data (black and white) and simulated data (red and blue) in (a). (e-f) Same as (c-d) for data simulated in (b).*